High Quantum Efficiency Uni-Traveling-Carrier Photodiode

Jizhao Zang, Zhanyu Yang, Xiaojun Xie, Min Ren, Yang Shen, Zack Carson, Olivier Pfister, Andreas Beling, and Joe C. Campbell, *Fellow, IEEE*

***Abstract*— We report uni-traveling-carrier photodiodes with a quantum efficiency of 98% ±0.8% at 1064 nm. For 50 μm devices, the measured 3-dB bandwidth is 2 GHz and the dark current is 10 nA at a bias voltage of −5 V. The dark current is dominated by generation-recombination at a bias voltage of −10 V and the activation energy is 0.23 eV. At higher bias voltage, tunneling becomes a significant component of the dark current.**

***Index Terms*— Photodiode, quantum efficiency, quantum information, uni-travelling-carrier.**

I. Introduction

HIGH-QUANTUM-EFFICIENCY photodiodes are key components in quantum information and quantum optical systems [1]–[4]. The two most common approaches to increase the quantum efficiency are to employ a resonant-cavity-enhanced (RCE) structure or to increase the thickness of the absorbing region. For RCE photodiodes a thin absorption region is located inside a Fabry–Perot cavity [5]–[7]. The incident light at the resonant wavelength reflects back and forth in the cavity, which effectively increases the optical absorption length. Since a thinner absorber enables shorter transit-time, this structure has the potential for high bandwidth without degrading the quantum efficiency [8]. However, RCE detectors tend to be more complex than a single pass detector and they achieve high quantum efficiency in a narrow spectral range. The most straightforward method to achieve high quantum efficiency is simply to increase the thickness of the absorber [9]. On the other hand, if the layer is too thick, recombination can become a limiting factor. Therefore, it is important to optimize the thickness for the material at the operating wavelength. It is also important to incorporate a high-quality anti-reflection coating.

It is well known that a thick absorber results in a transit-time penalty. Thus high quantum efficiency is achieved at the cost of reduced bandwidth. The employment of uni-traveling-carrier (UTC) structures [10] is expected to compensate this transit-time penalty. But most of the reported UTC photodiodes are primarily designed for high frequency response.

Manuscript received October 14, 2016; revised December 3, 2016; accepted December 29, 2016. Date of publication January 4, 2017; date of current version January 25, 2017. This work was supported by the Defense Advanced Research Projects Agency through the QUINESS Program.

J. Zang, Z. Yang, X. Xie, M. Ren, Y. Shen, A. Beling, and J. C. Campbell are with the Department of Electrical and Computer Engineering, University of Virginia, Charlottesville, VA 22904 USA (e-mail: jcc7s@virginia.edu).

Z. Carson and O. Pfister are with the Department of Physics, University of Virginia, Charlottesville, VA 22903 USA (e-mail: op6n@virginia.edu).

Color versions of one or more of the figures in this letter are available online at http://ieeexplore.ieee.org.

Digital Object Identifier 10.1109/LPT.2016.2647638

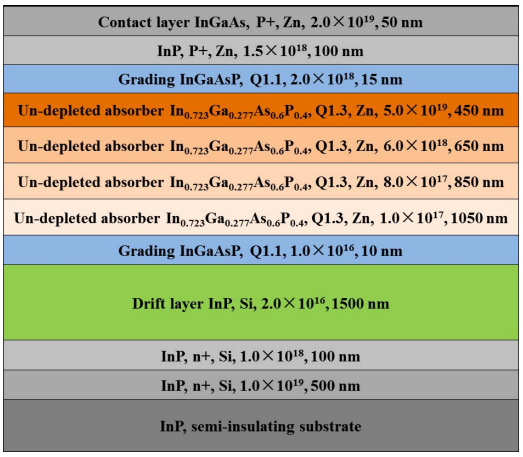

Fig. 1. Epitaxial-layer design of the high efficiency photodiode.

Typically, the quantum efficiency is relatively low due to the thin absorber. In [11], quantum efficiency of 66% (responsivity of 0.83 A/W at 1550 nm) was achieved by using a back-to-back mesa structure. It was reported in [12] that modified UTC photodiodes on silicon-on-insulator (SOI) waveguides achieved quantum efficiency of 76% (responsivity of 0.95 A/W at 1550 nm). These photodiodes were designed to operate at 1550 nm. However, for quantum optical systems, 1064 nm is often the preferred wavelength because it is the wavelength of Nd:YAG lasers, which are ultra-stable and low noise.

In this letter, we report high-quantum-efficiency uni-traveling-carrier (UTC) photodiodes that achieve 98% ±0.8% detection efficiency at 1064 nm. For 50 μm-diameter devices, the 3 dB bandwidth is 2 GHz, which is transit-time limited. Since the dark current is also important for applications in quantum optics, the current-voltage curves at different temperature are investigated.

II. Device Design and Fabrication

The epitaxial-layer structure of the photodiode is shown in Fig. 1. The epitaxial-layers were grown on semi-insulating InP substrate by metal organic chemical vapor deposition. Silicon and zinc are used as n-type and p-type dopants, respectively. The first layer grown is a 500 nm heavily n-doped (1×10^{19} cm^{-3}) contact layer. This is followed by a 100 nm (1×10^{18} cm^{-3}) n-doped InP layer. The drift layer is (2×10^{16} cm^{-3}) n-doped with a thickness of 1500 nm, which is designed to reduce the junction capacitance and obtain larger RC-limited bandwidth. After the drift layer, a 10 nm lightly doped InGaAsP quaternary layer is deposited

to assist electron transport and suppress carrier accumulation in the heterojunction interface. To fully absorb the light, the absorber is 3 μm-thick p-type $In_{0.723}Ga_{0.277}As_{0.6}P_{0.4}$, which is step-graded ($1\times10^{17}$ cm^{-3}, 8×10^{17} cm^{-3}, 6×10^{18} cm^{-3}, 5×10^{19} cm^{-3}) to create a quasi-field that aids carrier transport. The absorber cannot be too thick; otherwise the quantum efficiency will decrease due to •bandwidth. Given absorption coefficient of 2×10^{4} cm^{-1} [13], 99.75% of the incident light will be absorbed by the 3 μm-thick absorber, which is already enough for achieving high quantum efficiency. After the absorber, there is a 15 nm-thick InGaAsP grading layer to "smooth" the heterojunction discontinuity. Finally, the two top layers are a 100 nm 1.5×10^{18} cm^{-3}p-doped InP electron-blocking layer and a 50 nm heavily p-doped 2×10^{19} cm^{-3} InGaAs contact layer.

In photodiodes, both electron and hole currents exist, but their balance can be adjusted by the layer arrangement. For the traditional p-i-n structure, at high incident power, the electrical field in the depletion region may collapse due to the accumulated excess carrier densities (space charge). This results in compression of the output power, which is referred to as saturation. To increase the saturation power, we optimized the layer design based on the uni-travelling-carrier structure, in which the un-depleted absorber is very close to the cathode. The majority-carrier holes generated in the absorber will be collected in the dielectric relaxation time. Only electrons traverse the whole structure. Since the drift velocity of electrons is higher than that of holes, the space charge effect can be mitigated to enable higher output power. In addition, the lower transit-time associated with the electron velocity results in higher bandwidth.

The fabrication process begins with electron beam evaporation of the metal on the p-type InGaAs contact layer. Then SiO_2 is deposited in a plasma-enhanced chemical vapor deposition (PECVD) system and used as the etching mask. After photolithography and inductively coupled plasma (ICP) etching, the p-mesa pattern on the optical mask is transferred to the InGaAsP/InP layers. The dry etching is terminated in the highly doped n-contact layer and the same method is used for n-mesa etching. The SiO_2 mask layer on the n-mesa is removed by another photolithography process and wet etching with buffered oxide etchant (BOE). This is followed by the n-contact metal deposition. Finally, both ICP dry etching and BOE wet etching are used to remove the SiO_2 on the p-contact.

Since the metal on the p-mesa will block the incident light, the photodiode is designed for back illumination. To reduce the scattering and reflection at the semiconductor/air interface, the backside of the device was polished and coated with an anti-reflection coating (Evaporated Coatings Inc.). As shown in Fig. 2, the reflection spectrum is relatively narrow ($< 1\%$ from 1020 nm to 1125 nm) and centered at 1064 nm where the reflectivity is 0.012%.

III. Results and Discussion

Fig. 3(a) shows the experimental setup for quantum efficiency measurements. A tungsten-halogen lamp is used as a broadband optical source, followed by a monochromator to select specific wavelengths. A chopper is placed after the monochromator to provide intensity modulation (200-300 Hz). The light is collimated and then focused on the backside of the devices. Finally, the photocurrent is measured by a Stanford Research SR-850 lock-in amplifier.

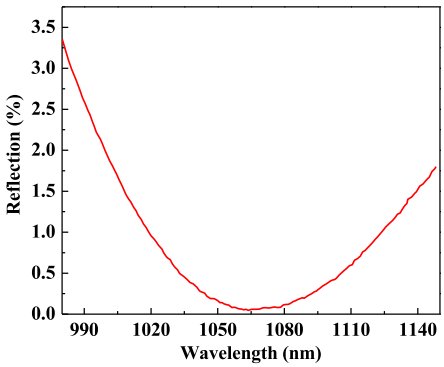

Fig. 2. Measured reflection versus wavelength after deposition of the anti-reflection coating.

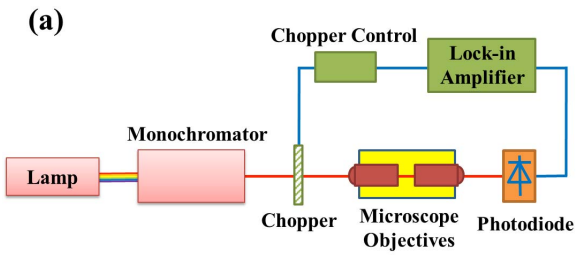

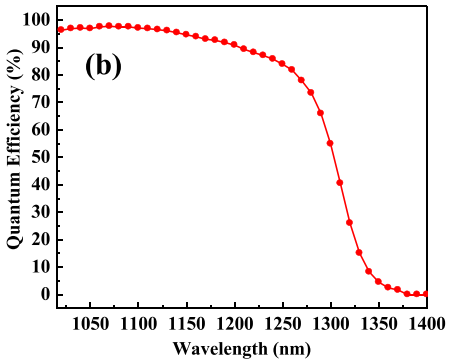

Fig. 3. (a) Quantum efficiency measurement setup; (b) measured quantum efficiency of a device with diameter of 250 μm. The bias voltage is -5 V.

Four diameters were fabricated (50 μm, 125 μm, 250 μm, 350 μm). Fig. 3(b) is the measured quantum efficiency of a 250 μm device at -5 V. Since device size will not influence the quantum efficiency, all kinds of devices should have the same efficiency. The quantum efficiency is $> 90\%$ in the wavelength range 1000 nm to 1200 nm. At 1064 nm, the measured quantum efficiency is 98% $\pm$0.8%. Approximately 0.5% of the incident light is absorbed by the InP substrate, and 0.4% is reflected at the interface of InP drift layer and InGaAsP grading layer. Recombination in the absorber accounts for a loss of 1.1%. The band gap energy of the absorber material, $In_{0.723}Ga_{0.277}As_{0.6}P_{0.4}$, is 0.96 eV and the corresponding cutoff wavelength is 1290 nm. Therefore, the quantum efficiency decreases quickly when

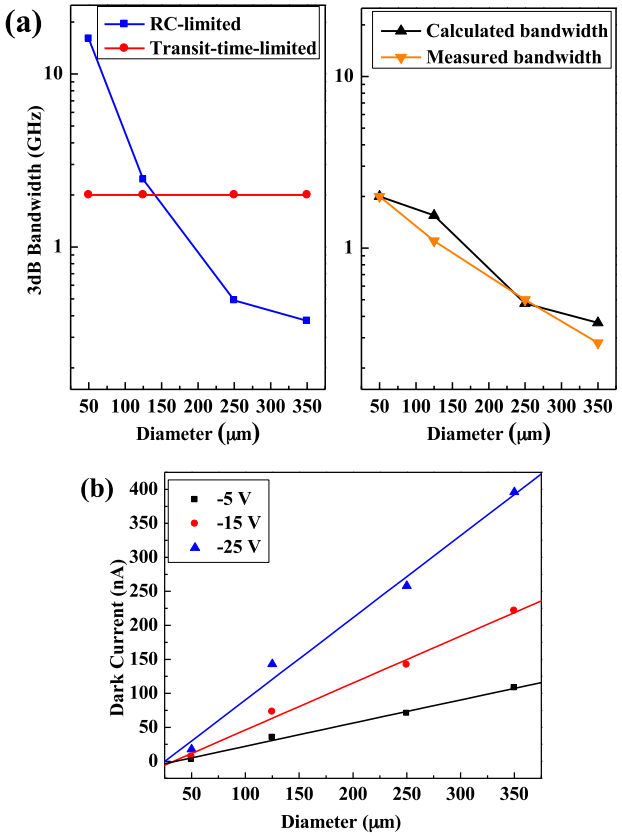

Fig. 4. (a) Calculated and measured bandwidth versus diameter at bias voltage of −5 V; (b) dark current versus diameter at different bias voltage.

the wavelength increases from 1250 nm to 1350 nm. For wavelengths less than 1064 nm, the quantum efficiency decreases slowly due to the narrow-band anti-reflection coating. When the wavelength changes from 1064 nm to 1020 nm, the reflection increases from 0.012% to ∼ 0.8%. If a broader-band anti-reflection coating were used, the quantum efficiency at shorter wavelength should be similar to that at 1064 nm. When the optical power is below 6 mW, the quantum efficiency is 98%. Above 6 mW average power, the quantum efficiency begins to decrease. At 10.5 mW, the quantum efficiency is 95%.

To measure the bandwidth, the devices were flip-chip bonded onto an AlN submount [14]. Fig. 4(a) shows the calculated and measured bandwidth for diameters in the range 50 μm to 350 μm at bias voltage of −5 V. Due to the unavailability of a laser or modulator at 1064 nm, the bandwidth was measured at 1250 nm. The measured bandwidth of the 50 μm device is 2 GHz. The ■ symbols show the calculated RC-limited bandwidth. The series resistance was extracted from the current-voltage curves and the capacitance was measured with an LCR meter. For the 50 μm devices, the RC-limited bandwidth (16 GHz) is much higher than the measured bandwidth, an indication of transit-time limited response. The transit time is independent of diameter as shown by the • symbols. The symbols, ▲, show the calculated bandwidth, including both RC and transit time effects. It can been seen that the calculated results agree well with the measured results, ▼. For 250 μm and 350 μm devices, the

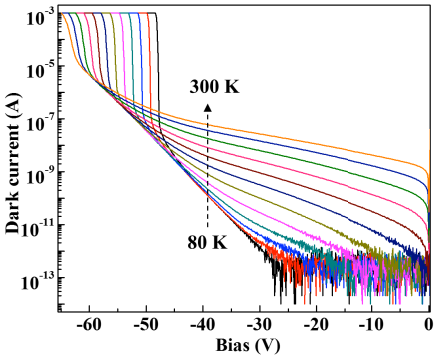

Fig. 5. Current-voltage curves of a 50 μm device for temperature 80 K to 300 K in 20 K steps.

bandwidth is lower than the transit-time-limited bandwidth, viz., RC-limited.

In our measurement, when the bias voltage is increased from −5 V to −15 V, the measured bandwidth does not change very much. Crosslight simulation shows that the depletion width is essentially unchanged. The electric field increases with bias but the junction capacitance is essentially constant. At −5 V, the electrical field is high enough that the carriers travel at the saturation velocity. It follows that the bandwidth will not change appreciably regardless of whether it is RC or transit-time limited.

In quantum optical systems, the dark current of the photodiodes is one of the primary concerns. It needs to be as low as possible to reduce the noise. In addition, some of the entangled photon signals will be extremely low power (∼45 nA per pulse). As a result the dark current needs to be low enough to accurately measure them. Fig. 4(b) shows the dark current versus device diameter. Since the dark current varies linearly with diameter, it can be concluded that surface leakage dominates.

Fig. 5 shows the measured current-voltage curves of a 50 μm-diameter device in the temperature range 80 K to 300 K in steps of 20 K. At 300 K and lower bias voltage (0 to −25 V), the dark current is in the range 10-100 nA, and decreases with temperature. As expected the avalanche breakdown voltage increases with temperature owing to the fact that, when the temperature increases, the mean free path of the carrier decreases due to increased phonon scattering. Therefore, a higher electrical field is required to ensure that the carriers have sufficient kinetic energy to initiate the avalanche breakdown process.

The temperature dependence of the dark current versus voltage can be used to identify the dominated physical mechanisms. There are two primary sources of the dark current, generation-recombination and band-to-band tunneling. The temperature dependence of generation-recombination is given by the expression [15]:

$$I_{dark} \propto T^2 e^{-\frac{E_a}{k_b T}} \quad (1)$$

where E_a is activation energy and k_b is the Boltzmann constant. A plot of $-\ln(I_{dark}/T^2)$ versus $1/k_bT$ is linear if the dark current is dominated by generation-recombination. On the other hand the same plot will exhibit exponential decay if the dark current is dominated by tunneling. Fig. 6(a) shows

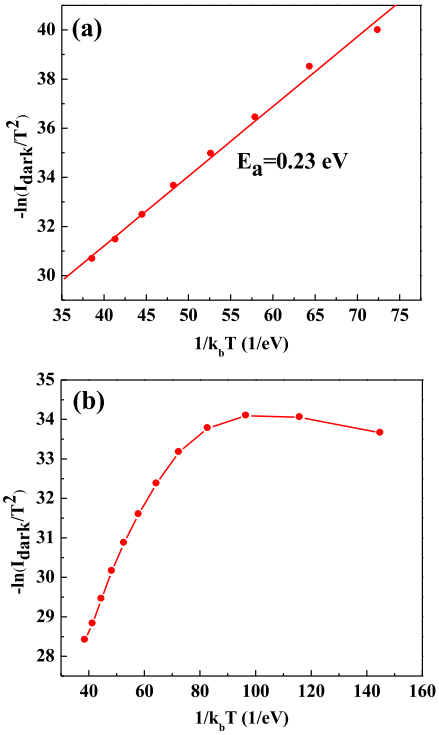

Fig. 6. $-\ln(I_{dark}/T^2)$ versus $1/k_bT$ for a 50 μm–diameter device at (a) -10 V and (b) -35 V.

$-\ln(I_{dark}/T^2)$ versus $1/k_bT$ when the bias voltage is -10V. The slope indicates that the dark current is dominated by generation-recombination and the activation energy is 0.23 eV. The same curve at bias voltage of -35 V is shown in Fig. 6(b). The nonlinearity of this curve indicates that band-to-band tunneling becomes significant at temperatures below 140 K.

IV. Conclusion

In this letter, we report UTC photodiodes with 98% $\pm$0.8% external quantum efficiency at 1064 nm. To achieve high quantum efficiency, a 3-μm-thick absorber was utilized to fully absorb the light. Surface polishing and anti-reflection coating effectively reduced the scattering and reflection at the semiconductor/air interface. At bias voltage of -5 V, the 3 dB bandwidth is 2 GHz and the dark current is 10 nA. The dark current at low bias voltage is dominated by generation-recombination with 0.23 eV activation energy.

References

[1] R. Bloomer, M. Pysher, and O. Pfister, "Nonlocal restoration of two-mode squeezing in the presence of strong optical loss," *New J. Phys.*, vol. 13, p. 063014, Jun. 2011.

[2] M. Pysher, R. Bloomer, C. M. Kaleva, T. D. Roberts, P. Battle, and O. Pfister, "Broadband amplitude squeezing in a periodically poled $KTiOPO_4$ waveguide," *Opt. Lett.*, vol. 34, no. 3, pp. 256–258, Feb. 2009.

[3] A. R. Wade *et al.*, "A squeezed light source operated under high vacuum," *Sci. Rep.*, vol. 5, p. 18052, Dec. 2015.

[4] H. Vahlbruch, M. Mehmet, K. Danzmann, and R. Schnabel, "Detection of 15 dB squeezed states of light and their application for the absolute calibration of photoelectric quantum efficiency," *Phys. Rev. Lett.*, vol. 117, p. 110801, Sep. 2016.

[5] A. G. Dentai, R. Kuchibhotla, J. C. Campbell, C. Tsai, and C. Lei, "High quantum efficiency, long wavelength InP/InGaAs microcavity photodiode," *Electron. Lett.*, vol. 27, no. 23, pp. 2125–2127, Nov. 1991.

[6] E. Özbay *et al.*, " High-speed >90% quantum-efficiency p–i–n photodiodes with a resonance wavelength adjustable in the 795–835 nm range," *Appl. Phys. Lett.*, vol. 74, no. 8, pp. 1072–1074, Feb. 1999.

[7] I. Kimukin, N. Biyikli, B. Butun, O. Aytur, S. M. Unlu, and E. Özbay, "InGaAs-based high-performance p-i-n photodiodes," *IEEE Photon. Technol. Lett.*, vol. 14, no. 3, pp. 366–368, Mar. 2002.

[8] M. S. Ünlü and S. Strite, "Resonant cavity enhanced photonic devices," *J. Appl. Phys.*, vol. 78, no. 2, pp. 607–639, Jul. 1995.

[9] X. Li *et al.*, "A partially depleted absorber photodiode with graded doping injection regions," *IEEE Photon. Technol. Lett.*, vol. 16, no. 10, pp. 2326–2328, Oct. 2004.

[10] T. Ishibashi, S. Kodama, N. Shimizu, and T. Furuta, "High-speed response of uni-traveling-carrier photodiodes," *Jpn. J. Appl. Phys.*, vol. 36, no. 10, pp. 6263–6268, Oct. 1997.

[11] T. Shi, B. Xiong, C. Sun, and Y. Luo, "Novel back-to-back uni-traveling-carrier photodiodes with high responsivity and wide bandwidth," in *Proc. Opt. Fiber Commun. Conf.*, 2013, p. OW3J.2.

[12] X. Xie *et al.*, "Heterogeneously integrated waveguide-coupled photodiodes on SOI with 12 dBm output power at 40 GHz," in *Proc. Opt. Fiber Commun. Conf.*, 2015, p. Th5B.7.

[13] H. Burkhard, H. W. Dinges, and E. Kuphal, "Optical properties of $In_{1-x}Ga_xP_{1-y}As_y$, InP, GaAs, and GaP determined by ellipsometry," *J. Appl. Phys.*, vol. 53, no. 1, pp. 655–662, Jan. 1982.

[14] X. Xie *et al.*, "Photonic generation of high-power pulsed microwave signals," *J. Lightw. Technol.*, vol. 33, no. 18, pp. 3808–3814, Sep. 15, 2015.

[15] W. Sun *et al.*, "High-Gain InAs Avalanche Photodiodes," *IEEE J. Quantum Electron.*, vol. 49, no. 2, pp. 154–161, Feb. 2013.